CLEO CONF95-24

EPS0188

June 30, 1995

MEASUREMENTS OF THE ELECTROMAGNETIC TRANSITION FORM FACTORS OF LIGHT PSEUDOSCALAR MESONS AT A LARGE MOMENTUM TRANSFER

D.M. Asner,[1] M. Athanas,[1] D.W. Bliss,[1] W.S. Brower,[1] G. Masek,[1] H.P. Paar,[1] M. Sivertz,[1] J. Gronberg,[2] C.M. Korte,[2] R. Kutschke,[2] S. Menary,[2] R.J. Morrison,[2] S. Nakanishi,[2] H.N. Nelson,[2] T.K. Nelson,[2] C. Qiao,[2] J.D. Richman,[2] D. Roberts,[2] A. Ryd,[2] H. Tajima,[2] M.S. Witherell,[2] R. Balest,[3] K. Cho,[3] W.T. Ford,[3] M. Lohner,[3] H. Park,[3] P. Rankin,[3] J.G. Smith,[3] J.P. Alexander,[4] C. Bebek,[4] B.E. Berger,[4] K. Berkelman,[4] K. Bloom,[4] T.E. Browder,[4*] D.G. Cassel,[4] H.A. Cho,[4] D.M. Coffman,[4] D.S. Crowcroft,[4] M. Dickson,[4] P.S. Drell,[4] D.J. Dumas,[4] R. Ehrlich,[4] R. Elia,[4] P. Gaidarev,[4] R.S. Galik,[4] M. Garcia-Sciveres,[4] B. Gittelman,[4] S.W. Gray,[4] D.L. Hartill,[4] B.K. Heltsley,[4] S. Henderson,[4] C.D. Jones,[4] S.L. Jones,[4] J. Kandaswamy,[4] N. Katayama,[4] P.C. Kim,[4] D.L. Kreinick,[4] T. Lee,[4] Y. Liu,[4] G.S. Ludwig,[4] J. Masui,[4] J. Mevissen,[4] N.B. Mistry,[4] C.R. Ng,[4] E. Nordberg,[4] J.R. Patterson,[4] D. Peterson,[4] D. Riley,[4] A. Soffer,[4] P. Avery,[5] A. Freyberger,[5] K. Lingel,[5] C. Prescott,[5] J. Rodriguez,[5] S. Yang,[5] J. Yelton,[5] G. Brandenburg,[6] D. Cinabro,[6] T. Liu,[6] M. Saulnier,[6] R. Wilson,[6] H. Yamamoto,[6] T. Bergfeld,[7] B.I. Eisenstein,[7] J. Ernst,[7] G.E. Gladding,[7] G.D. Gollin,[7] M. Palmer,[7] M. Selen,[7] J.J. Thaler,[7] K.W. Edwards,[8] K.W. McLean,[8] M. Ogg,[8] A. Bellerive,[9] D.I. Britton,[9] E.R.F. Hyatt,[9] R. Janicek,[9] D.B. MacFarlane,[9] P.M. Patel,[9] B. Spaan,[9] A.J. Sadoff,[10] R. Ammar,[11] P. Baringer,[11] A. Bean,[11] D. Besson,[11] D. Coppage,[11] N. Copty,[11] R. Davis,[11] N. Hancock,[11] S. Kotov,[11] I. Kravchenko,[11] N. Kwak,[11] Y. Kubota,[12] M. Lattery,[12] M. Momayezi,[12] J.K. Nelson,[12] S. Patton,[12] R. Poling,[12] V. Savinov,[12] S. Schrenk,[12] R. Wang,[12] M.S. Alam,[13] I.J. Kim,[13] Z. Ling,[13] A.H. Mahmood,[13] J.J. O'Neill,[13] H. Severini,[13] C.R. Sun,[13] F. Wappler,[13] G. Crawford,[14] R. Fulton,[14] D. Fujino,[14] K.K. Gan,[14] K. Honscheid,[14] H. Kagan,[14] R. Kass,[14] J. Lee,[14] M. Sung,[14] C. White,[14] A. Wolf,[14] M.M. Zoeller,[14] X. Fu,[15] B. Nemati,[15] W.R. Ross,[15] P. Skubic,[15] M. Wood,[15] M. Bishai,[16] J. Fast,[16]

E. Gerndt,[16] J.W. Hinson,[16] T. Miao,[16] D.H. Miller,[16] M. Modesitt,[16] E.I. Shibata,[16] I.P.J. Shipsey,[16] P.N. Wang,[16] L. Gibbons,[17] S.D. Johnson,[17] Y. Kwon,[17] S. Roberts,[17] E.H. Thorndike,[17] T.E. Coan,[18] J. Dominick,[18] V. Fadeyev,[18] I. Korolkov,[18] M. Lambrecht,[18] S. Sanghera,[18] V. Shelkov,[18] T. Skwarnicki,[18] R. Stroynowski,[18] I. Volobouev,[18] G. Wei,[18] M. Artuso,[19] M. Gao,[19] M. Goldberg,[19] D. He,[19] N. Horwitz,[19] S. Kopp,[19] G.C. Moneti,[19] R. Mountain,[19] F. Muheim,[19] Y. Mukhin,[19] S. Playfer,[19] S. Stone,[19] X. Xing,[19] J. Bartelt,[20] S.E. Csorna,[20] V. Jain,[20] S. Marka,[20] D. Gibaut,[21] K. Kinoshita,[21] P. Pomianowski,[21] B. Barish,[22] M. Chadha,[22] S. Chan,[22] D.F. Cowen,[22] G. Eigen,[22] J.S. Miller,[22] C. O'Grady,[22] J. Urheim,[22] A.J. Weinstein,[22] and F. Würthwein[22]

(CLEO Collaboration)

[1] *University of California, San Diego, La Jolla, California 92093*

[2] *University of California, Santa Barbara, California 93106*

[3] *University of Colorado, Boulder, Colorado 80309-0390*

[4] *Cornell University, Ithaca, New York 14853*

[5] *University of Florida, Gainesville, Florida 32611*

[6] *Harvard University, Cambridge, Massachusetts 02138*

[7] *University of Illinois, Champaign-Urbana, Illinois, 61801*

[8] *Carleton University, Ottawa, Ontario K1S 5B6 and the Institute of Particle Physics, Canada*

[9] *McGill University, Montréal, Québec H3A 2T8 and the Institute of Particle Physics, Canada*

[10] *Ithaca College, Ithaca, New York 14850*

[11] *University of Kansas, Lawrence, Kansas 66045*

[12] *University of Minnesota, Minneapolis, Minnesota 55455*

[13] *State University of New York at Albany, Albany, New York 12222*

[14] *Ohio State University, Columbus, Ohio, 43210*

[15] *University of Oklahoma, Norman, Oklahoma 73019*

[16] *Purdue University, West Lafayette, Indiana 47907*

[17] *University of Rochester, Rochester, New York 14627*

[18] *Southern Methodist University, Dallas, Texas 75275*

[19] *Syracuse University, Syracuse, New York 13244*

[20] *Vanderbilt University, Nashville, Tennessee 37235*

[21] *Virginia Polytechnic Institute and State University, Blacksburg, Virginia, 24061*

[22] *California Institute of Technology, Pasadena, California 91125*

ABSTRACT

Using the CLEO-II detector, we have studied the exclusive two-photon production of the light pseudoscalar mesons in the single-tagged mode. We report on preliminary measurements of the π^0, η and η' electromagnetic transition form factors in the Q^2 region from 2.0 (GeV/c)^2 to 20.0 (GeV/c)^2.

---

[*] Permanent address: University of Hawaii at Manoa

The processes discussed in this report are

$$e^+e^- \rightarrow e^+e^- \ (\pi^0/\eta/\eta').$$

To lowest order in quantum electrodynamics perturbation theory these processes are described as single-meson production by two space-like photons, one emitted by each electron. In our experiment we detect the decay products of the meson and one scattered electron which is referred to as the "tag". The other electron is scattered only at a small angle and remains undetected (*un*tagged). We measure the meson-production rates as a function of the momentum transfer, Q^2, which can be expressed in terms of the detected electron energy and scattering angle:

$$Q^2 \equiv -q^2 = 2E_\mathrm{b}E_\mathrm{t}(1-\cos\theta_\mathrm{t}).$$

Here E_b and E_t are the energies of the tagged electron before (*i.e.* energy of the beam) and after the scattering, and θ_t is the scattering angle. The study of the deviation of the meson-production rate from that which is predicted for a point-like meson gives a form factor measurement. Previous experiments[1,2,3] have measured the $\eta\gamma^*\gamma$-transition form factor in the Q^2 region below 3.4 $(\mathrm{GeV/c})^2$. Statistically significant measurements[2,3] of the η' electromagnetic form factor in the space-like region exist for Q^2 below 3.4 $(\mathrm{GeV/c})^2$. Our study furnishes information in Q^2 range from 2.0 $(\mathrm{GeV/c})^2$ to 12.0 $(\mathrm{GeV/c})^2$ for the η and from 2.0 $(\mathrm{GeV/c})^2$ to 20.0 $(\mathrm{GeV/c})^2$ for the η'. The only measurement of the π^0 form factor in the space-like region[3] is limited to Q^2 below 2.7 $(\mathrm{GeV/c})^2$. We have measured the $\pi^0\gamma^*\gamma$-transition form factor in the region of Q^2 from 3.0 $(\mathrm{GeV/c})^2$ to 8.0 $(\mathrm{GeV/c})^2$. In our analysis we study the π^0, η and η' form factors using the following decay channels: $\pi^0 \rightarrow \gamma\gamma$; $\eta \rightarrow \gamma\gamma$, $\eta \rightarrow \pi^+\pi^-\pi^0$ $(\pi^0 \rightarrow \gamma\gamma)$; $\eta' \rightarrow \rho^0\gamma$ and $\eta' \rightarrow \pi^+\pi^-\eta$ $(\eta \rightarrow \gamma\gamma)$.

The measurements described here utilize data collected with the CLEO-II general purpose magnetic detector.[4] It is operated at the Cornell Electron Storage Ring (CESR) which is a symmetric e^+e^- collider running at the center of mass energy around 10.6 GeV. We have analysed data corresponding to an e^+e^- integrated luminosity of 2.88 fb^{-1}. In the CLEO-II detector, charged particle trajectories are measured with a set of three concentric cylindrical drift chambers located inside a 1.5-Tesla solenoidal magnetic field. They cover 95% of the solid angle, with momentum resolution

$$\sigma_p/p(\%) = \sqrt{(0.15p)^2 + (0.50)^2} \quad (p \ \text{ in GeV/c}).$$

The electromagnetic calorimeter consists of 7800 thalium-doped CsI scintillation crystals and is used for photon detection and electron identification. The relative energy and angular resolution (in mrad) of the calorimeter are shown below.
In the barrel part:

$$\sigma_E/E(\%) = 0.35/E^{0.75} + 1.9 - 0.1E, \quad \sigma_\phi = 2.8/\sqrt{E} + 2.5, \quad \sigma_\theta = 0.8\ \sigma_\phi\ \sin\theta,$$

and in the endcap part:

$$\sigma_E/E(\%) = 0.26/E + 2.5, \quad \sigma_\phi = 3.7/\sqrt{E} + 7.3, \quad \sigma_\theta = 1.4/\sqrt{E} + 5.6,$$

where photon energy E is in GeV. The calorimeter covers 98% of the solid angle. The time-of-flight (TOF) system covering 97% of the solid angle consists of scintillation counters and is an important part of the trigger system.

The trigger system[5] of the CLEO-II detector consists of ten triggers suitable for different physics processes. In our analysis we use data collected with two of these triggers. The first trigger requires that both the tagged electron and the decay products of π^0, η or η' meson are detected. The signature of the tagged electron consists of track segments reconstructed by a fast track-finding processor, a hit in the TOF system and a shower of at least 500 MeV. In order to identify the decay products of the meson another shower of energy above 500 MeV or two separated showers (of at least 200 MeV of deposited energy each) must be found in the barrel part of the calorimeter. The other trigger we use requires at least two tracks, one with momentum transverse to the beam line ($p^\perp$) above 400 MeV/c and the other with $p^\perp$ above 200 MeV/c. In addition, hits in two non-adjacent TOF counters and two separated energy clusters (above 200 MeV each) must be found in the barrel part of the detector. For one-prong events (when no charged hadrons are produced in the decay of the meson) we limit our analysis to tagged electrons detected exclusively in the endcap calorimeter, where the trigger efficiency for these events is well understood. For three-prong events (when the tagged electron and two charged pions are detected) the uncertainty in the trigger efficiency is reduced even when the tag is outside the endcap calorimeter since we use both of the above mentioned triggers simultaneously.

To measure the energy and the scattering angle of the tagged electron we employ the following techniques:

- The magnitude of the transverse (to the beam axis) momentum of the tag ($p_{\rm t}^\perp$) is assumed to be equal to the $p_{\rm h}^\perp$, where $p_{\rm h}^\perp$ is a magnitude of the transverse momentum of the hadronic system. To calculate the momentum ($\vec{p}_{\rm h}$) and the energy ($E_{\rm h}$) of the hadronic system we use momenta and energies of all detected particles except the tag. All charged tracks are assumed to be produced by pions. All neutral clusters of more than 30 MeV of deposited energy in the barrel part and of more than 50 MeV in the endcap part of the calorimeter are identified as electromagnetic showers produced by photons originating from the event vertex (for the one-prong events it coincides with the nominal interaction point). To be identified as a neutral cluster no charged tracks should be found near the cluster; *i.e.* the angle between directions to the centroid of the cluster and to the impact point of any charged particle with the calorimeter must be larger than $20°$ as viewed from the event vertex.

- The tag scattering angle, $\theta_{\rm t}$, is measured from the centroid of the shower associated with the tag rather than using the angle of the poorly reconstructed charged track. Tag identification is described later.

- The energy and momentum of the tag ($\vec{p}_{\rm t}$) are obtained using the azimuthal location of the shower, $\theta_{\rm t}$ and $p_{\rm t}^{\perp}$. Since shower leakage at small angles is significant, this method gives a better $E_{\rm t}$ resolution than the endcap calorimeter energy measurement.

Event selection criteria are designed to isolate two-photon events where the only missing particle is the *un*tagged electron of high momentum. To select an event we require that the following conditions be satisfied:

- A tag candidate is identified: both a charged track and a cluster (of energy above 1 GeV) are found. The cluster centroid and the projected track impact point agree to within $20°$ when viewed from the interaction point. We assume this cluster to be an electromagnetic shower produced by the tag.

- The hadronic system has no net charge, *i.e.* $\sum q_i = 0$ (excluding the charged track produced by a tag candidate).

- The *un*tagged electron is scattered at an angle below $20°$. This angle is determined from the direction of the missing momentum ($\vec{p}_{\rm m}$) which we assume to be due solely to the *un*tagged electron. The missing momentum is defined as follows:

$$\vec{p}_{\rm m} = -(\vec{p}_{\rm t} + \vec{p}_{\rm h})$$

- The magnitude of the missing momentum ($|\vec{p}_{\rm m}|$) and the missing energy ($E_{\rm m} = 2E_{\rm b} - E_{\rm h} - E_{\rm t}$) satisfy the following criteria:

$$2.0 \text{ GeV} \leq E_{\rm m} \leq 6.0 \text{ GeV}$$
$$2.0 \text{ GeV/c} \leq |\vec{p}_{\rm m}| \leq 6.0 \text{ GeV/c}$$
$$-2.0 \text{ GeV} \leq (E_{\rm m} - |\vec{p}_{\rm m}|) \leq 2.0 \text{ GeV}$$

(in the $\eta \to \pi^+\pi^-\pi^0$ analysis we apply a tighter hermeticity requirement on ($E_{\rm m} - |\vec{p}_{\rm m}|$) which is discussed later).

- Three-prong events have a unique photon pair with a mass within 3σ of the nominal η or π^0 mass where σ is the experimental resolution. To achieve the best possible resolution in Q^2 a full kinematic fit is performed for this photon pair where it is constrained to have exactly the η or π^0 mass. We assume that all other neutral clusters are produced by hadrons interacting strongly in the material of the detector. The total energy deposited into these other neutral clusters should not exceed 300 MeV.

- One-prong events contain exactly two electromagnetic showers in the barrel part of the calorimeter. No showers are found in the endcap part of the calorimeter.

- Finally, in the $\pi^0 \to \gamma\gamma$ and $\eta \to \gamma\gamma$ analyses photon energies should not be very asymmetric, *i.e.* $\cos\theta^* < 0.9$. Here θ^* is the angle between higher-energy photon momentum calculated in the $\gamma\gamma$ center of mass frame and the momentum of the $\gamma\gamma$ system calculated in the laboratory frame. The need for this requirement is discussed later.

We show the distributions of the hadronic-system masses for the events satisfying the above selection criteria in Figs. 1, 2 and 3. The background under the π^0 signal

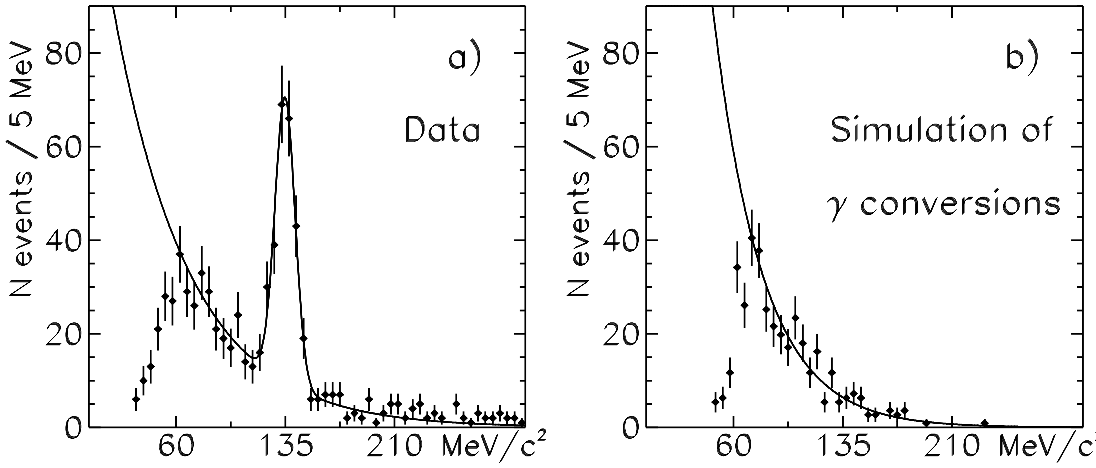

Fig. 1. The $\gamma\gamma$ mass distributions for a) the data events and b) the radiative Bhabha simulation events. The radiative photon conversion occurs in the material of the drift chamber. An arbitrary normalization is performed to compare only shape of the distribution in data and simulation. Description of the fits can be found in the text.

peak in Fig. 1a comes primarily from radiative Bhabha events *i.e.* $e^+e^- \to e^+e^-\gamma$. There are two mechanisms with which the radiative Bhabha events contribute to the background. First, an electromagnetic shower caused by a single photon of high energy can be occasionally accompanied by a low energy noise cluster. Since cluster energies in these background events are highly asymmetric, they congregate near $\cos\theta^* = 1$. Most of these events are rejected by requiring that $\cos\theta^* < 0.9$ in one-prong analyses. In the decays of the π^0 and η mesons the distribution of $\cos\theta^*$ is flat.

Second, some radiative Bhabha events contribute to the $\gamma\gamma$ mass plot if a γ converts

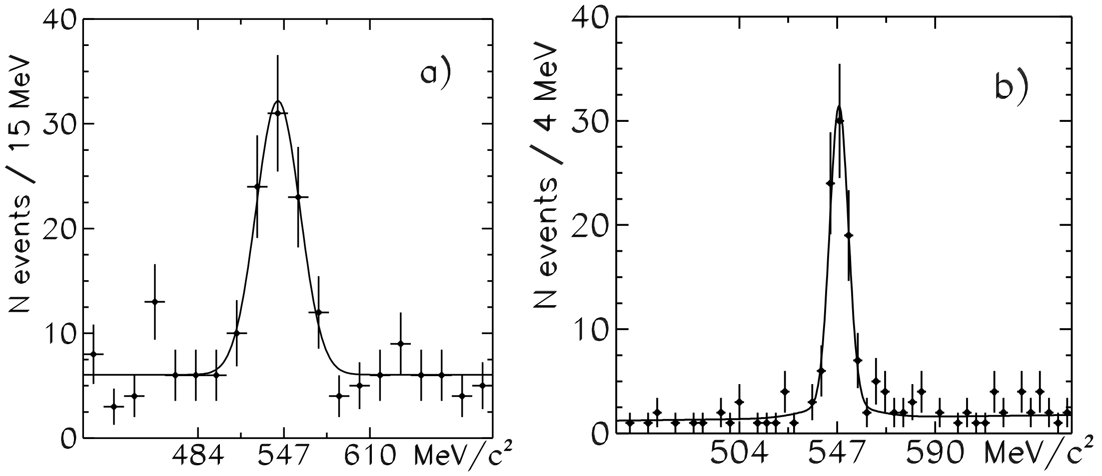

Fig. 2. The mass distributions for the a) $\eta \to \gamma\gamma$ and b) $\eta \to \pi^+\pi^-\pi^0$ ($\pi^0 \to \gamma\gamma$; photons are constrained to have exactly the π^0 mass) signals. The fits are described in the text.

into an e^+e^- pair in the outer layers of the drift chamber. The magnetic field causes a spatial separation of the produced pair and the electromagnetic showers developed in the calorimeter are indistinguishable from the showers caused by real photons when no tracks are reconstructed. This is confirmed by an extensive visual scan of selected data events. In addition, we have studied the photon conversion in the material of the detector by running a GEANT-based detector simulation program. The results of this study are consistent with our understanding of this background. The $\gamma\gamma$ mass plot for simulated single-photon radiative Bhabha events is shown in Fig. 1b and is well described by an exponential.

To obtain the number of events in the signal peak we fit the data distribution shown in Fig. 1a with a Gaussian for the signal and an exponential for the remaining background. We observe 211 ± 18 signal events in the $\pi^0 \to \gamma\gamma$ decay mode. In the $\eta \to \gamma\gamma$ analysis we fit the mass distribution shown in Fig. 2a with a Gaussian for the signal, and a flat background and observe 74 ± 11 signal events.

For three-prong analyses the signal-shape functions are obtained by running the detector simulation program. For the $\eta \to \pi^+\pi^-\pi^0$ ($\pi^0 \to \gamma\gamma$) and the $\eta' \to \pi^+\pi^-\eta$ ($\eta \to \gamma\gamma$) analyses we fit the simulated signal with a combination of two Gaussians with different widths and the same peak position. This reflects the variation of the detector resolution over the angular and energy ranges of the decay products. In the $\eta' \to \rho^0\gamma$ analysis the resolution function has a distinctive radiative tail due to the energy leakage from the shower produced by a photon. We obtain the values of the parameters of these signal-shape functions from the simulations and use them to fit the data distributions. The combinatoric background contributions which appear under the η and η' signals shown in Figs. 2b, 3a and 3b are approximated as linear. The numbers of signal events obtained from the fits to the data distributions are: 85 ± 10 in the $\eta \to \pi^+\pi^-\pi^0$ ($\pi^0 \to \gamma\gamma$), 211 ± 16 in the $\eta' \to \pi^+\pi^-\eta$ ($\eta \to \gamma\gamma$) and 373 ± 36 in the $\eta' \to \rho^0\gamma$ analyses.

The most serious backgrounds arise from events which include real π^0, η or η'. These backgrounds would peak in the mass distribution plots shown in Figs. 1, 2 and 3 if some of the final-state particles are not detected. For example, $e^+e^- \to e^+e^-\pi^0\pi^0$ events in which one π^0 is lost in the beam direction will appear as $e^+e^- \to e^+e^-\pi^0$. In order to estimate this background we have run extensive simulations of different two-photon processes. Typically our simulation sample size exceeds our data by a factor of 30. So far, we have found that $e^+e^- \to e^+e^-\eta'$ followed by $\eta' \to \eta\pi^0\pi^0$ is the only process which feeds several events into our $\eta \to \pi^+\pi^-\pi^0$ signal. In order to suppress this background a more restrictive hermeticity cut is applied in the $\eta \to \pi^+\pi^-\pi^0$ analysis:

$$-0.6 \text{ GeV} \leq (E_{\text{m}} - |\vec{p}_{\text{m}}|) \leq 0.6 \text{ GeV}.$$

According to our simulation the discussed background is suppressed by a factor of 7, while the event reconstruction efficiency is reduced by a factor of 1.15.

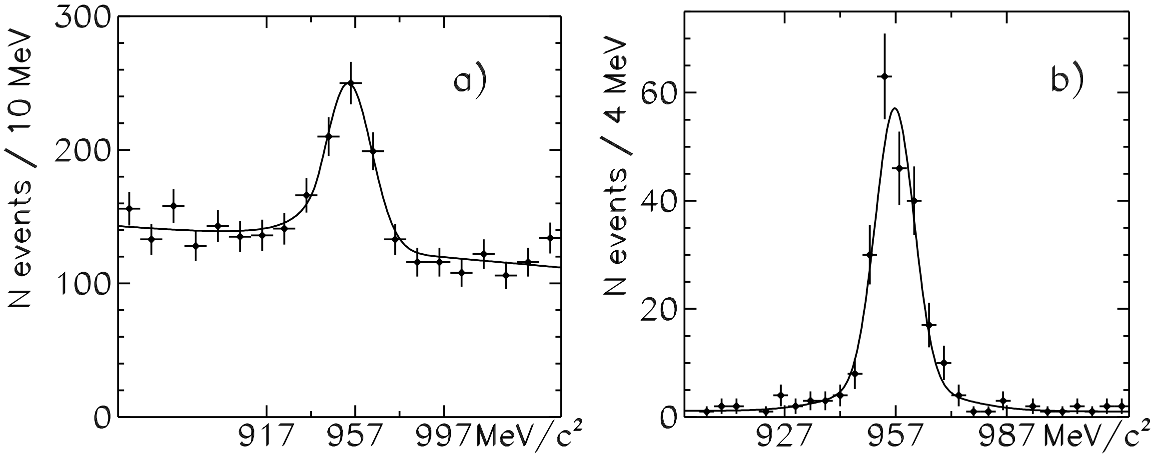

Fig. 3. The mass distributions for the a) $\eta' \to \rho^0\gamma$ and b) $\eta' \to \pi^+\pi^-\eta$ ($\eta \to \gamma\gamma$; photons are constrained to have exactly the η mass) signals. Fits are described in the text.

Simulations have been also performed for the single-photon annihilation processes, *i.e.* $e^+e^- \to \gamma^* \to$ lepton pairs or hadrons. We can make an independent estimate of the possible contribution from these processes using the correlation between the charge of the tagged electron and the direction of the missing momentum. In two-photon signal events the *un*tagged electron (positron) is scattered at a very small angle and travels along the direction of the original electron (positron) beam. Thus, the direction of the missing momentum uniquely determines the charge of the tag.

This is not the case for the single-photon annihilation events. The observed rate for events with a "wrong" charge of the tag is consistent with the charge misidentification probability of $\approx 0.5\%$ measured using endcap Bhabha events. This implies that the background from the annihilation processes is negligible.

Electro-production of a meson in the field of a beam-gas nucleus is also a possible source of background. We estimate this background using distributions of the event vertex position along the beam line and $x = (E_{\rm h} + E_{\rm t})/E_{\rm b}$ which are shown in Fig. 4. Beam-gas events peak at $x = 1.0$ and are uniformly distributed from -20 cm to +20 cm along the beam line as measured from the nominal interaction point. From the number of events in the tails of the distributions we conclude that beam-gas contamination is insignificant.

The total contribution from all background processes associated with resonance production (*i.e.* not fully reconstructed events and beam-gas interactions) is estimated to be below 1 event in each channel studied.

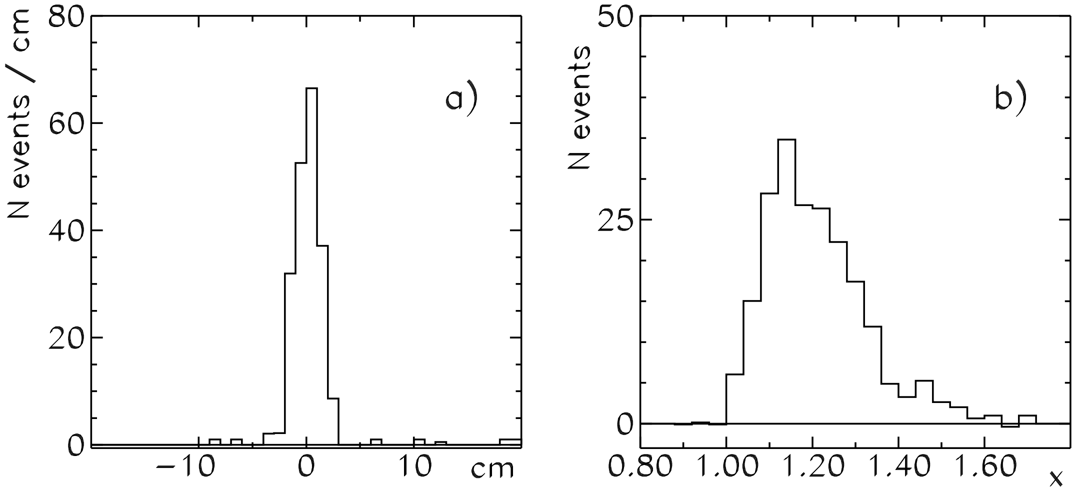

Fig. 4. a) The position of the event vertex along the beam line for the $\eta' \to \pi^+\pi^-\eta$ ($\eta \to \gamma\gamma$) signal events, b) $x = (E_{\rm h} + E_{\rm t})/E_{\rm b}$ for the $\pi^0 \to \gamma\gamma$ signal events (background subtracted using sidebands in the mass distributions).

To obtain the event reconstruction efficiency we use simulation programs based on the formalism of Budnev[6] with a simple double-pole vector meson dominance (VMD) form factor model.[7] We measure trigger efficiencies and estimate their uncertainties using redundancies between different triggers in data (*e.g.* by comparing efficiencies of the trigger based on the energy deposited into the electromagnetic calorimeter and the triggers based on the fast track-finding processors and TOF system). In addition, we compare measured trigger efficiencies with trigger simulation results. The detection efficiencies which include both the event reconstruction and the trigger efficiencies are obtained in bins of Q^2. As examples, these efficiencies are shown in

Fig. 5 for the $\pi^0 \to \gamma\gamma$ and $\eta' \to \pi^+\pi^-\eta$ $(\eta \to \gamma\gamma)$ analyses. The poor detection efficiency at low Q^2 is due to the vanishing geometrical acceptance of our detector at small θ_t and limitations imposed by the trigger system which requires that a cluster of ≈ 500 MeV or higher be detected in the endcap calorimeter. Taking into account that at least some of the decay products of the hadronic system must be found in the barrel part of the detector we effectively select events with tags of energy above ≈ 1 GeV. In our detector electrons can be tagged in the endcap CsI electromagnetic calorimeter when they are scattered at angles larger than 16.5°. Our analysis is limited to tags scattered at angles larger than 20° for one-prong events and larger than 24° for three-prong events where the trigger efficiency has been extensively studied. For three-prong modes the detection efficiency at $Q^2 > 12.0$ $(\mathrm{GeV/c})^2$ decreases due to the lower trigger efficiency when the tag is outside the endcap part of the calorimeter. For one-prong mode the detection efficiency is vanishing at high Q^2 due to the requirement that the tag is found in the endcap part of the electromagnetic calorimeter.

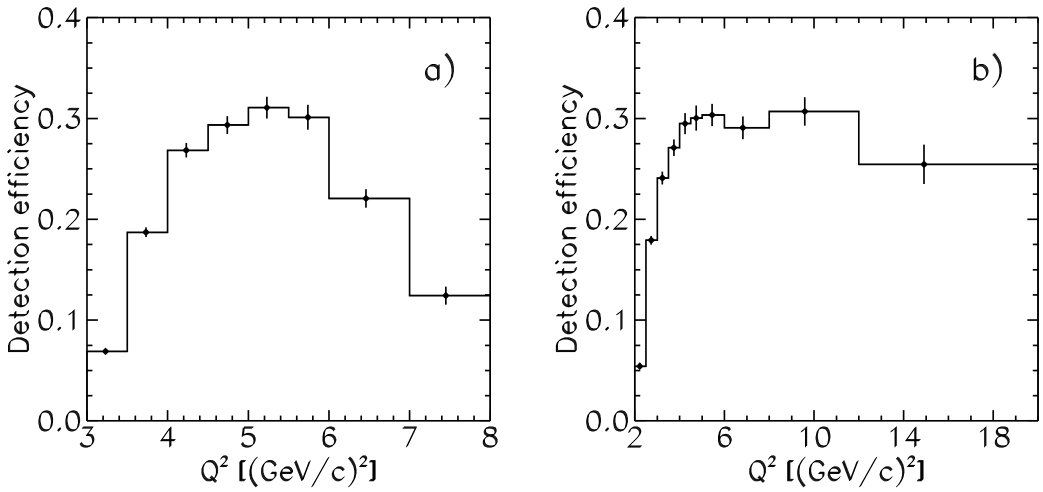

Fig. 5. The detection efficiency as a function of Q^2 for a) the $\pi^0 \to \gamma\gamma$ and b) the $\eta' \to \pi^+\pi^-\eta$ $(\eta \to \gamma\gamma)$ analyses.

We extract the Q^2 dependence of the form factor by comparing the measured production rate with that which is predicted for point-like pseudoscalar mesons. Our preliminary results are shown in Figs. 6, 7 and 8. Each bin center in Q^2 is determined from the weighted average of the theoretical Q^2 distribution inside this bin assuming that the VMD model is correct. We interpret our results in terms of Λ_p, the mass parameter which describes Q^2 development of the form factor for pseudoscalar meson "p". This parameter Λ_p is obtained by fitting our data with a function of the following form:

$$|\mathcal{F}(Q^2, q^2)|^2 \times M^3/64\pi = \Gamma_{\gamma\gamma}/(1 + Q^2/\Lambda_p^2)^2$$

Table I. Summary of the results on the pole mass Λ_p [MeV], describing the momentum transfer dependence of the form factors and the f_p [MeV], pseudoscalar meson coupling constant. Errors shown are statistical. See text for description of systematic uncertainties.

	Lepton-G[1]	TPC/2γ [2]	CELLO[3]	CLEO (this study)
Λ_{π^0}			748 ± 30	771 ± 18
Λ_η	720 ± 90	700 ± 80	839 ± 63	787 ± 23
$\Lambda_{\eta'}$		850 ± 70	794 ± 44	821 ± 15
f_{π^0}			84 ± 3	87 ± 2
f_η	81 ± 10	91 ± 6	94 ± 7	89 ± 3
$f_{\eta'}$		78 ± 5	89 ± 5	92 ± 2

Here $\mathcal{F}(Q^2, q^2)$ is the electromagnetic transition form factor which is a function of Q^2 and q^2 (the momentum transfer due to the photon emitted by the *un*detected electron), M is the mass of the meson "p" and $\Gamma_{\gamma\gamma}$ is its two-photon partial width (7.35 eV, 0.463 keV and 4.3 keV for the π^0, η and η', respectively).[8] We estimate the unmeasured momentum transfer q^2 to be below 0.001 $(\mathrm{GeV/c})^2$ using simulations, and ignore this effect in our analyses, assuming $q^2 = 0$. Since the numbers of events observed in the different decay channels of the η (η') meson are comparable, the fit is performed to both experimental distributions shown in Figs. 2a and 2b (3a and 3b) simultaneously.

It is predicted[9] that in the asymptotic limit ($Q^2 \to \infty$) the pole mass can be expressed in terms of the pseudoscalar meson coupling constant f_p as $f_p^2 = \Lambda_p^2/(8\pi^2)$. A summary of our results on the Λ_p and f_p and a comparison with the previous measurements are shown in Table I. Note that the errors quoted in this table are only statistical. Sources of the systematic error of our experiment include trigger and detector simulation, tracking, variation in the event selection criteria and background estimates. Taken in quadrature, uncertainties of our measurement correspond to a relative systematic error of 5% for one-prong and of 10% for three-prong events. An additional source of a relative systematic error of 5% is the uncertainty in the measured values of $\Gamma_{\gamma\gamma}$.

In summary, we report preliminary results of the analysis of electromagnetic transition form factors of the light pseudoscalar mesons π^0, η and η' in the space-like region. In terms of the pole mass fit and decay coupling constant our results are consistent with previous measurements but with improved precision. For the first time π^0 and η form factors are measured at Q^2 above 2.7 and 3.4 $(\mathrm{GeV/c})^2$, respectively. Also, this is the first statistically significant measurement for the η' at Q^2 above 3.4 $(\mathrm{GeV/c})^2$.

We gratefully acknowledge the effort of the CESR staff in providing us with excellent luminosity and running conditions. This work was supported by the National Science Foundation, the U.S. Department of Energy, the Heisenberg Foundation, the Alexander von Humboldt Stiftung, the Natural Sciences and Engineering Research Council of Canada, and the A.P. Sloan Foundation.

1. R.I. Djhelyadin *et al.*, Lepton-G Exp., *Phys. Lett.* **B94** (1980) 548.
2. H. Aihara *et al.*, TPC/2γ Coll., *Phys. Rev. Lett.* **64** (1990) 172.
3. H.-J. Behrend *et al.*, CELLO Coll., *Z. Phys.* **C49** (1991) 401.
4. Y. Kubota *et al.*, CLEO Coll., *Nucl. Inst. and Meth.* **A320** (1992) 66.
5. C. Bebek *et al.*, CLEO Coll., *Nucl. Inst. and Meth.* **A302** (1992) 261.
6. V.M. Budnev *et al.*, *Phys. Rep.* **C15** (1975) 181.
7. See, for example, M. Poppe, *Int. J. Mod. Phys.* **1** (1986) 545.
8. Review of Particle Properties, *Phys. Rev.* **D50** (1994) 1.
9. S.J. Brodsky and G.P. Lepage, *Phys. Rev.* **D24** (1981) 1808.

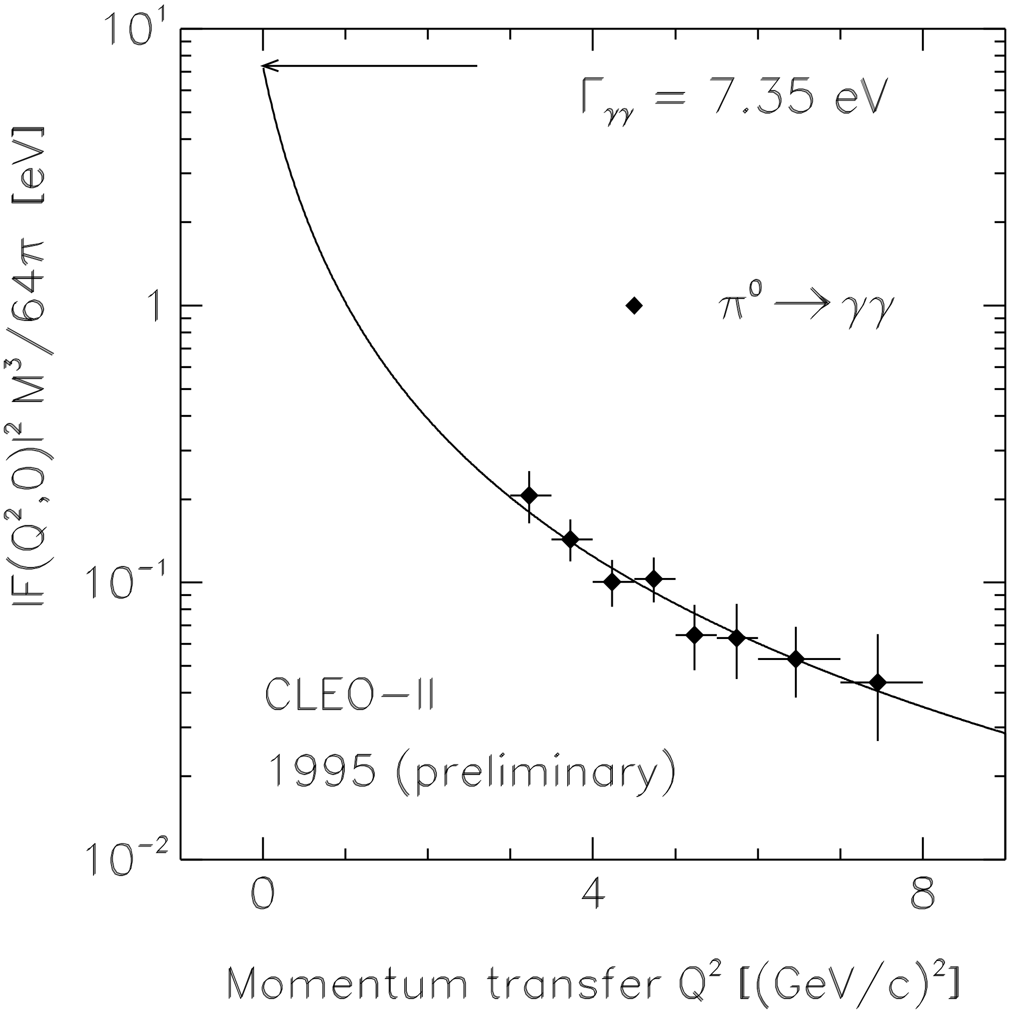

Fig. 6. The π^0 meson form factor. The pole mass fit is described in the text.

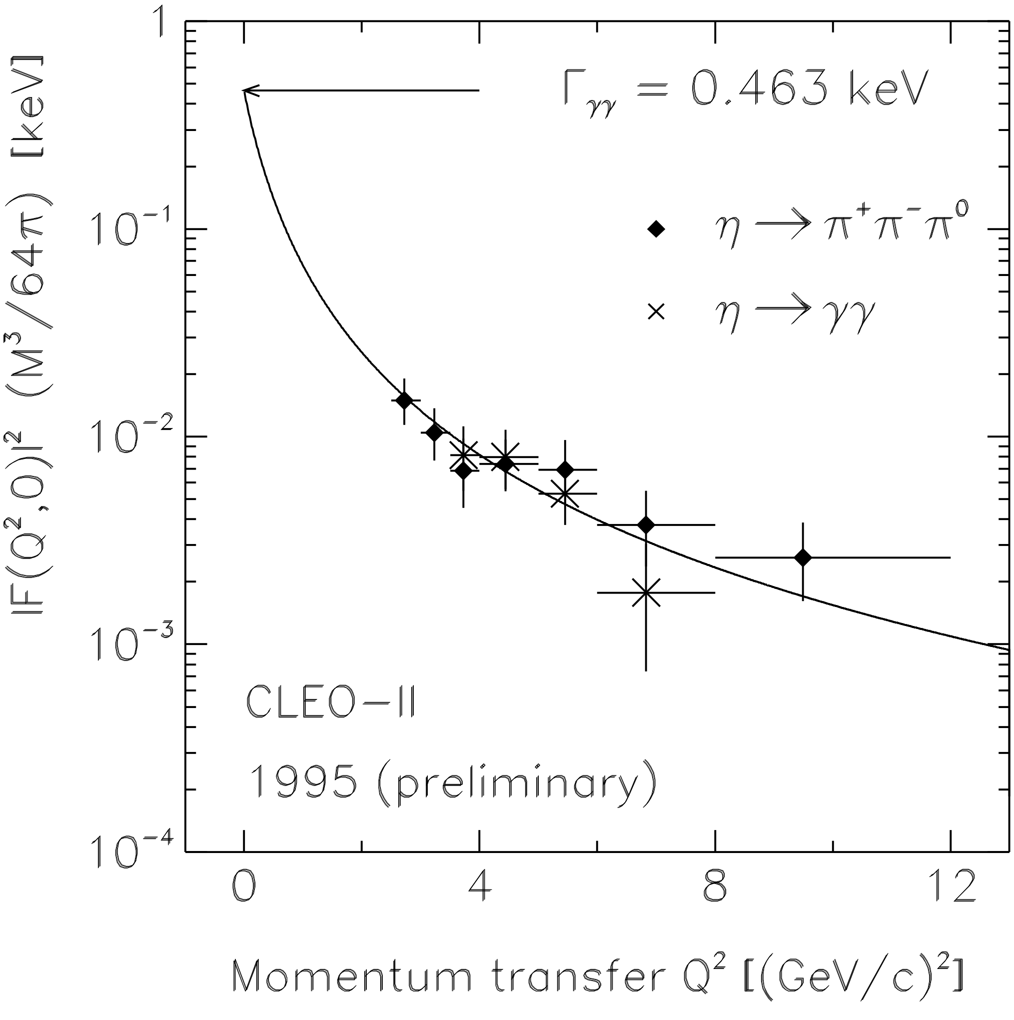

Fig. 7. The η meson form factor. The pole mass fit is described in the text.

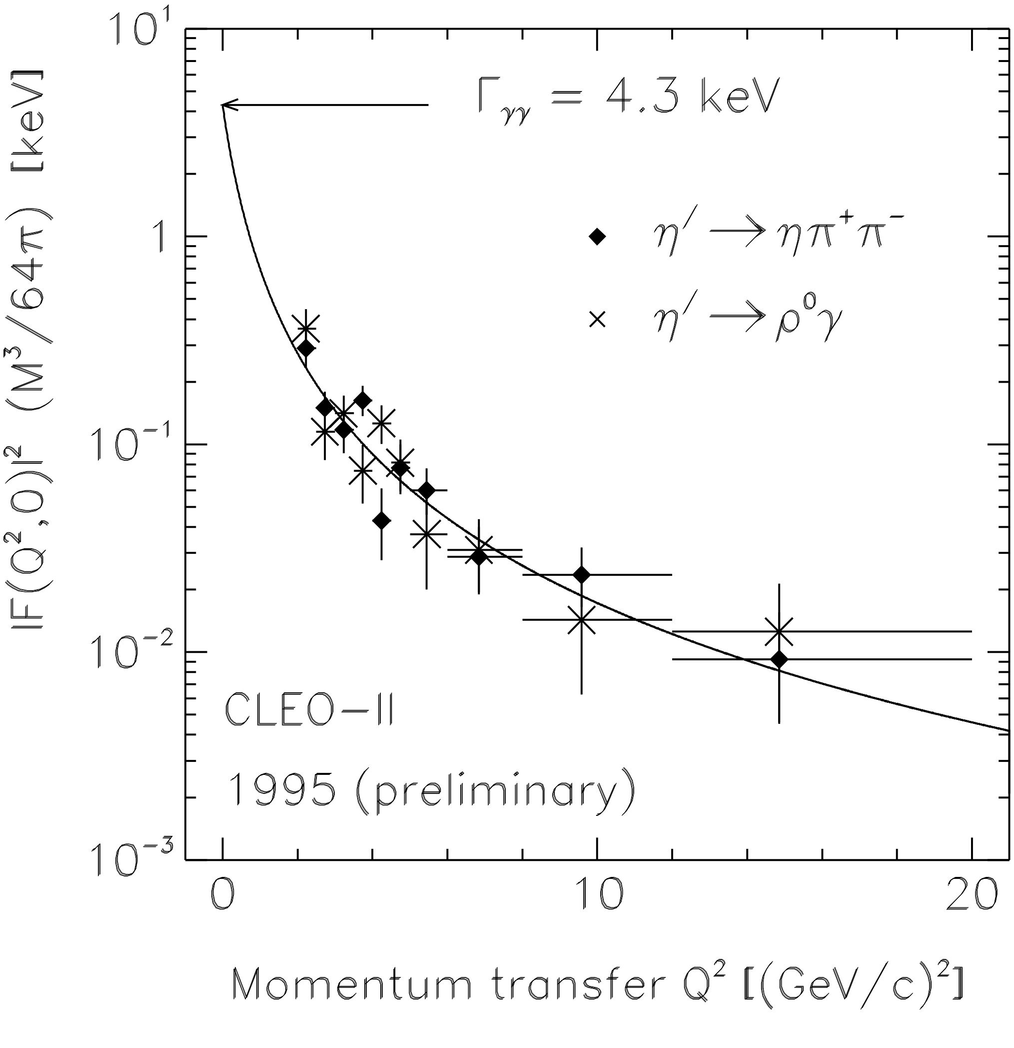

Fig. 8. The η' meson form factor. The pole mass fit is described in the text.